Volume 23
Number 14
14 April 2025
Pages 3233-3472

# Organic & Biomolecular Chemistry

rsc.li/obc

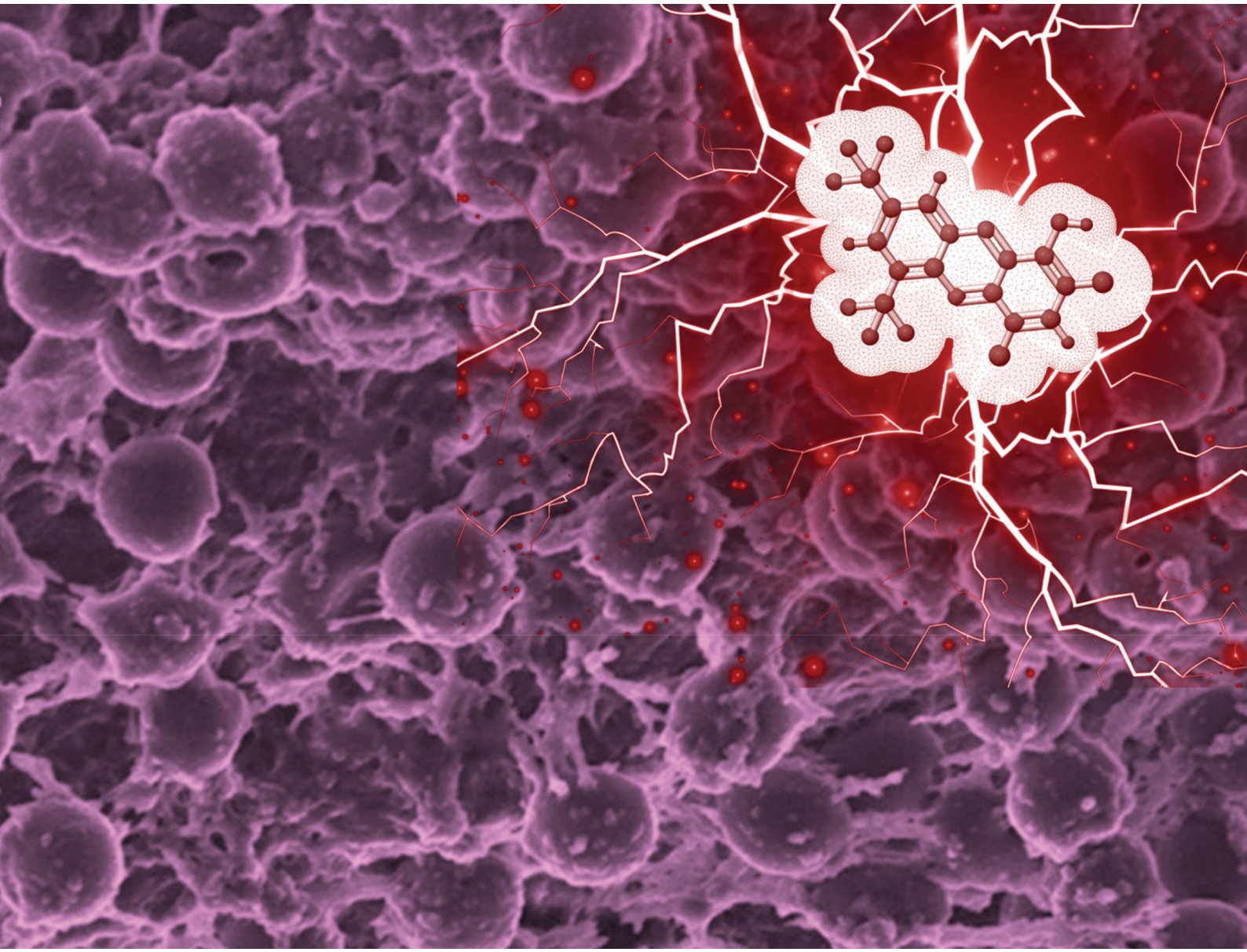

ISSN 1477-0520

ROYAL SOCIETY OF CHEMISTRY

**PAPER**
Robert W. Huigens III *et al.*
Identification of 6,8-ditrifluoromethyl halogenated phenazine as a potent bacterial biofilm-eradicating agent

Organic & Biomolecular Chemistry

ROYAL SOCIETY OF CHEMISTRY

PAPER

View Article Online
View Journal | View Issue

Open Access Article. Published on 06 January 2025. Downloaded on 2/6/2026 5:04:38 PM.
This article is licensed under a Creative Commons Attribution-NonCommercial 3.0 Unported Licence.

Check for updates

Cite this: *Org. Biomol. Chem.*, 2025, **23**, 3342

# Identification of 6,8-ditrifluoromethyl halogenated phenazine as a potent bacterial biofilm-eradicating agent†

Qiwen Gao,[a,b] Hongfen Yang,[b] Jeremy Sheiber,[c] Priscila Cristina Bartolomeu Halicki,[c] Ke Liu,[b] David Blanco,[b] Sadie Milhous,[b] Shouguang Jin,[d] Kyle H. Rohde,[c] Renee M. Fleeman[c] and Robert W. Huigens III *[a,b,e,f]

Bacterial biofilms are surface-attached communities consisting of non-replicating persister cells encased within an extracellular matrix of biomolecules. Unlike bacteria that have acquired resistance to antibiotics, persister cells enable biofilms to demonstrate innate tolerance toward all classes of conventional antibiotic therapies. It is estimated that 50–80% of bacterial infections are biofilm associated, which is considered the underlying cause of chronic and recurring infections. Herein, we report a modular three-step synthetic route to new halogenated phenazine (HP) analogues from diverse aniline and nitroarene building blocks. The HPs were evaluated for antibacterial and biofilm-killing properties against a panel of lab strains and multidrug-resistant clinical isolates. Several HPs demonstrated potent antibacterial (MIC ≤ 0.39 μM) and biofilm-eradicating activities (MBEC < 10 μM) with 6,8-ditrifluoromethyl-HP **15** demonstrated remarkable biofilm-killing potencies (MBEC = 0.15–1.17 μM) against Gram-positive pathogens, including methicillin-resistant *Staphylococcus aureus* clinical isolates. Confocal microscopy showed HP **15** induced significant losses in the polysaccharide matrix in MRSA biofilms. In addition, HP **15** showed increased antibacterial activities against dormant *Mycobacterium tuberculosis* (*Mtb*, MIC = 1.35 μM) when compared to replicating *Mtb* (MIC = 3.69 μM). Overall, this new modular route has enabled rapid access to an interesting series of potent halogenated phenazine analogues to explore their unique antibacterial and biofilm-killing properties.

Received 11th December 2024,
Accepted 5th January 2025

DOI: 10.1039/d4ob02011a

rsc.li/obc

[a]*Department of Pharmaceutical & Biomedical Sciences, College of Pharmacy, University of Georgia, Athens, Georgia 30602, USA. E-mail: Robert.Huigens@uga.edu, qiwen.gao@uga.edu; Tel: +706-542-7787*
[b]*Department of Medicinal Chemistry, Center for Natural Products, Drug Discovery and Development (CNPD3), College of Pharmacy, University of Florida, Gainesville, Florida 32610, USA. E-mail: yanghf88@gmail.com, liu_ke@gzlab.ac.cn, DBlanco5016@gmail.com, smilhous@unc.edu*
[c]*Division of Immunity and Pathogenesis, Burnett School of Biomedical Sciences, College of Medicine, University of Central Florida, Orlando, Florida 32827, USA. E-mail: je503372@ucf.edu, PriscilaCristina.BartolomeuHalicki@ucf.edu, kyle.rohde@ucf.edu, renee.fleeman@ucf.edu*
[d]*Department of Molecular Genetics & Microbiology, College of Medicine, University of Florida, Gainesville, Florida 32610, USA. E-mail: sjin3499@gmail.com*
[e]*Department of Chemistry, Franklin College of Arts and Sciences, University of Georgia, Athens, Georgia 30602, USA*
[f]*Department of Infectious Diseases, College of Veterinary Medicine, University of Georgia, Athens, Georgia 30602, USA*

†Electronic supplementary information (ESI) available: Supporting figures, characterization data for newly synthesized (with tabulated $^{1}$H & $^{13}$C NMR data, HRMS, melting points for solids, and NMR spectra), UV-vis spectroscopy results for iron(II) binding, microbiological assay results, cytotoxicity assay results, and HPLC traces with purity analysis for HPs synthesized and evaluated during these studies. See DOI: https://doi.org/10.1039/d4ob02011a

Bacterial infections have become increasingly challenging to treat with conventional antibiotics due to acquired resistance and innate tolerance.[1–3] Every class of clinically used antibiotic was initially discovered to inhibit rapidly-dividing planktonic bacteria. Unfortunately, pathogenic bacteria have acquired resistance to antibiotics through a multitude of mechanisms, including: target mutation or overexpression, efflux pump action, enzyme-mediated antibiotic inactivation, and altered membrane chemistry to decrease drug penetration.[3–6] In addition, individual (free-floating) planktonic bacteria utilize a sophisticated signaling system known as quorum sensing to communicate and coordinate group behaviors, including the attachment to a surface and subsequent biofilm formation (Fig. 1).[7] Bacterial biofilm communities consist of enriched populations of non-replicating persister cells encased within an extracellular polymeric matrix of polysaccharides, proteins, and extracellular DNA.[3,8,9] Due to their non-replicating phenotype, biofilms demonstrate high levels of innate antibiotic tolerance and are credited as the primary cause of chronic and recurring infections.[8,10–12]


This journal is © The Royal Society of Chemistry 2025

Open Access Article. Published on 06 January 2025. Downloaded on 2/6/2026 5:04:38 PM.
This article is licensed under a Creative Commons Attribution-NonCommercial 3.0 Unported Licence.

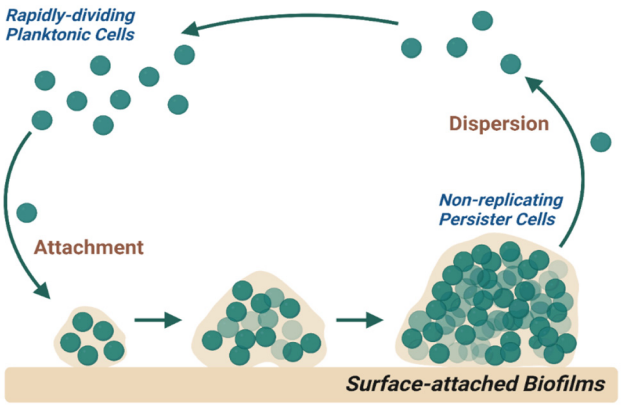


**Fig. 1** Individual, free-floating planktonic bacteria coordinate the simultaneous attachment to a surface where subsequent development leads to a mature biofilm community consisting of enriched populations of non-replicating (metabolically-dormant) persister cells. Established biofilms will disperse planktonic cells back into the surrounding environment and are credited as the underlying cause of chronic and recurring bacterial infection.

Despite an antibiotic pipeline that has struggled to produce clinically useful agents over the last ~50 years, innovative approaches have delivered exciting advances in recent years.[3,13–16] Lewis and colleagues have developed an incredible natural product-focused discovery platform that has resulted in (1) ClpP-activating agent ADEP4 that kills persister cells and eradicates a chronic biofilm infection in mice,[17] (2) the development of iChip technology that led to the identification of the lipid II and III binding antibiotic teixobactin from "unculturable" bacteria,[18] and (3) the discovery of darobactin, an antibiotic that targets BamA and kills Gram-negative pathogens, isolated from a nematode bacterial symbiont.[19] Myers and co-workers have developed robust total synthesis platforms to access new tetracyclines[20–24] (including FDA-approved eravacycline), macrolides,[25–28] clindamycins (iboxamycin, IBX, is a promising lead),[29] and a bridged macrobicyclic antibiotic cresomycin[30] designed to overcome multidrug-resistant pathogens. The Boger lab has reported new vancomycin analogues that (1) enable dual binding of transpeptidase's D-Ala–D-Ala (wild type) and D-Ala–D-Lac (vancomycin resistant) moiety, (2) results in transglycosylase inhibition, and (3) cause membrane permeabilization to overcome vancomycin resistance.[31–34] In recent years, the Hergenrother team has (1) defined predictive compound accumulation (eNTRy) rules to target Gram-negative pathogens,[35–39] (2) reported porin-independent accumulation rules for *Pseudomonas aeruginosa*,[40] and (3) discovered lolamicin, a Gram-negative-specific antibiotic targeting the lipoprotein transport system while sparing the gut microbiota in mice.[41] Smith, Heise, and colleagues at Genentech reported G0775, an optimized arylomycin, that inhibits the essential bacterial type I signal peptidase through covalent modification and demonstrates efficacy against Gram-negative pathogens in mouse models of infection.[42]

Our work to address problems associated with antibiotic-resistant and -tolerant pathogens has been inspired by the action of phenazine antibiotics.[43–45] Individuals suffering from cystic fibrosis (CF) are inflicted with chronic lung infections. Oftentimes, young CF patients are initially infected by *Staphylococcus aureus* and, as they age, *Pseudomonas aeruginosa* later co-infects their lungs. It is believed that *P. aeruginosa* secretes the redox-active phenazine pyocyanin in microbial warfare to kill *S. aureus* and become the primary pathogen infecting the CF patient's lungs.[46] As CF-related lung infections are chronic, we hypothesized that pyocyanin must play a role in eradicating *S. aureus* biofilms and initiated a research program to explore the antibacterial properties of phenazine molecules.

Initial efforts from our lab focused on the synthesis and antibacterial assessment (in minimum inhibitory concentration, or MIC assays) of 13 diverse phenazine antibiotics and synthetic phenazines.[47] We were encouraged to discover marine *Streptomyces* derived 2-bromo-1-hydroxyphenazine (MIC = 6.25 μM = 1.72 μg $mL^{-1}$) demonstrates significantly more potent antibacterial activities than pyocyanin (MIC = 50 μM = 10.5 μg $mL^{-1}$) against *S. aureus* and *S. epidermidis*.[47] In addition, we found synthetic analogue 2,4-dibromo-1-hydroxyphenazine (halogenated phenazine analogue 1, or **HP-1**; Fig. 2) to demonstrate potent planktonic growth inhibition (MIC = 1.56 μM = 0.55 μg $mL^{-1}$).[47] In other work, **HP-1** was shown to eradicate *S. aureus* biofilms at a minimum biofilm eradication concentration, or MBEC, value of 100 μM (35.4 μg $mL^{-1}$).[48]

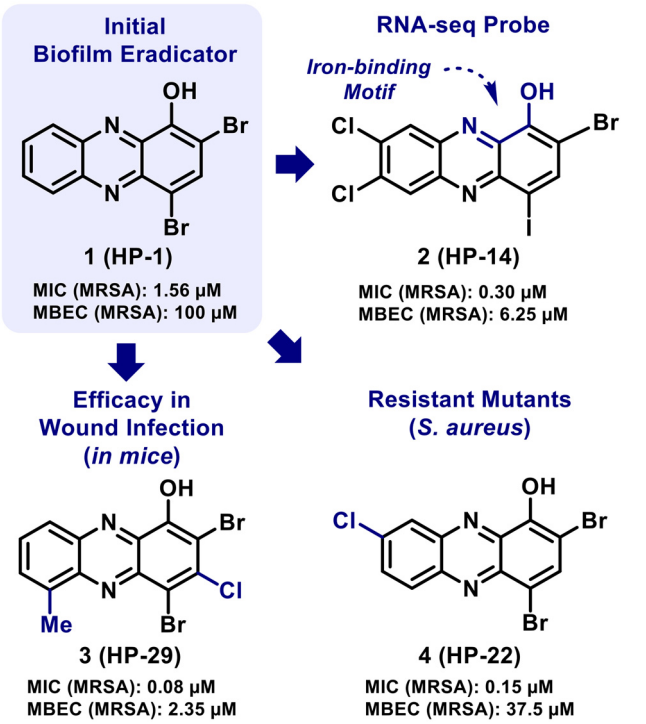


**Fig. 2** Halogenated phenazine (HP) analogues that have demonstrated potent biofilm eradication activities and/or have been used as probes to explore mechanistic insights.

Open Access Article. Published on 06 January 2025. Downloaded on 2/6/2026 5:04:38 PM.
This article is licensed under a Creative Commons Attribution-NonCommercial 3.0 Unported Licence.

Our more recent efforts related to HPs have focused on exploring structure–activity relationships (SAR), using select analogues as probes in mode of action studies, and treating wound infections in mice (Fig. 2).[49–54] These collective efforts have led to a detailed SAR of more than 150 HPs with the identification of several potent HP analogues that eradicate (kill) biofilms of Gram-positive pathogens (*e.g.*, *S. aureus*, *S. epidermidis*; MBEC ≤ 10 μM). In addition, key mechanistic insights were obtained from transcript profiling (RNA-seq) studies that revealed **HP-14** induces rapid iron starvation in MRSA biofilms through the direct binding of iron.[51] Additional work has shown potent HP analogues to induce rapid starvation in *Staphylococcal* biofilms using RT-qPCR of select iron uptake biomarkers (*e.g.*, *isdB*, *sbnC*, *sfaA*, MW0695).[53–55] In a separate study, an HP-resistant mutant was generated in *S. aureus* using **HP-22** that had a single amino acid change in transcriptional regulator TetR21 (Arg116Cys).[56] RNA-seq analysis showed the TetR21$^{R116C}$ mutant to have up-regulated the transcription of *hprS* (halogenated phenazine resistant protein of *S. aureus*) and HprS was discovered as an efflux pump for phenazines.[56] In addition, **HP-29** demonstrated good *in vivo* efficacy against *S. aureus* UAMS-1 and *E. faecalis* OG1RF in wound infection models in mice.[53]

In the present study, we developed a modular route to several new halogenated phenazines from diverse nitroarene and aniline building blocks. This focused collection of HP small molecules was evaluated against a panel of pathogens in standard antibacterial assays and Calgary Biofilm Device assays to determine biofilm eradication activities against lab strains and clinical isolates. From these studies, we identified 6,8-ditrifluoromethyl-HP **15** to be the most potent biofilm-eradicating HP small molecule to date. To determine its ability to kill other drug-tolerant bacterial pathogens, HP **15** was also evaluated against both replicating and dormant *Mycobacterium tuberculosis* (*Mtb*) cultures. Using confocal microscopy experiments, HP **15** showed significant impacts on the extracellular polysaccharide matrix of established MRSA biofilms.

## Chemical synthesis of diverse halogenated phenazines

We synthesized nine halogenated phenazines using a three-step route from simple aniline and nitroarene building blocks (Scheme 1). To access the phenazine core, an aniline and a nitroarene were reacted in the presence of potassium *tert*-butoxide to join these materials through a regioselective C–N bond formation that results in a nitroso intermediate (select nitroso compounds were characterized in the ESI;† however, most were taken directly to the next synthetic step without purification), which was directly subjected to *N*,*O*-bis(trimethylsilyl)acetamide (BSA) to yield diverse 1-methoxyphenazines in 27–48% yield (36% average yield). This modular phenazine synthesis was inspired by work done in the Wróbel lab,[57–60] which we previously reported to access HP **15**.[61] With the phenazine nucleus intact, 1-methoxyphenazines were then transformed into halogenated phenazines *via* a demethylation step using boron tribromide ($BBr_3$: 53–100% yield, 9 examples) or aluminum(III) chloride ($AlCl_3$: 91–95% yield, 2 examples), and a final bromination reaction with *N*-bromosuccinimide (NBS: 28–99% yield). Three halogenated phenazines in Scheme 1 have been reported by our lab (7-Cl-HP **10**, 7-$CF_3$-HP **14**, 6,8-$CF_3$-HP **15**)[52,54,61] and were included to evaluate the efficiency of this synthetic route while expanding our understanding of their biological activities.

## Antibacterial evaluation of halogenated phenazines

Following synthesis, we evaluated the HP analogues to determine their ability to inhibit planktonic growth in minimum inhibition concentration (MIC) assays. MIC values were determined for HPs against a panel of Gram-positive pathogens (lab strains and drug-resistant clinical isolates; see Table 1 and ESI Table 1†), replicating and dormant *Mycobacterium tuberculosis* cultures, and Gram-negative pathogens (ESI Table 2†). Although this collection of HPs demonstrated impressive antibacterial activities against the Gram-positive pathogens, the MIC profiles of **10**, **14**, and **15** have been reported[52,54,61] and served as comparators to benchmark activity for new HPs described during these studies. All 7-position substituted HPs reported herein demonstrated moderate to significant improvements in antibacterial activities (up to 30-fold more potent MIC values; Table 1) when compared to parent **HP-1** against methicillin-resistant *Staphylococcus aureus* (MRSA), methicillin-resistant *S. epidermidis* (MRSE), methicillin-sensitive *S. epidermidis* (MSSE), vancomycin-resistant *Enterococcus faecium* (VRE), multidrug-resistant *Enterococcus faecalis* (strain OG1RF), and *Streptococcus pneumoniae* strains.

Here, we report the activity profiles of all halogens substituted at the 7-position of the HP scaffold, which demonstrated potent antibacterial activities (MIC = 0.04–1.56 μM against most Gram-positive strains; Table 1; Fig. 3A and B). In most instances, 7-bromo-HP **11** and 7-iodo-HP **12** analogues report equipotent MIC values compared to 7-chloro-HP **10**; however, 7-fluoro-HP **9** typically reports MIC values that are up to 4-fold less potent when compared to the other halogens at the 7-position of the HP scaffold. HP analogue **13** bears a –$SCF_3$ group at the 7-position of the HP core and demonstrated highly potent activities against the Gram-positive strains (MIC = 0.04–0.78 μM). HP **17** contains a benzyl group at the 7-position of the HP scaffold and demonstrated potent antibacterial activities (MIC = 0.10–0.78 μM) against nearly all Gram-positive strains in the Table 1 panel. To probe the SAR of the highly potent 6,8-ditrifluoromethyl-HP agent **15** (MIC = 0.05–0.20 μM against Gram-positive pathogens), we synthesized HP analogue **16** bearing a 3-chlorine atom as the lone difference between analogues; however, **16** (MIC = 0.20–4.69 μM) lost considerable activities compared to HP **15** and we believe this trend could correlate with losses in water solubility.

 This journal is © The Royal Society of Chemistry 2025

Open Access Article. Published on 06 January 2025. Downloaded on 2/6/2026 5:04:38 PM.
This article is licensed under a Creative Commons Attribution-NonCommercial 3.0 Unported Licence.

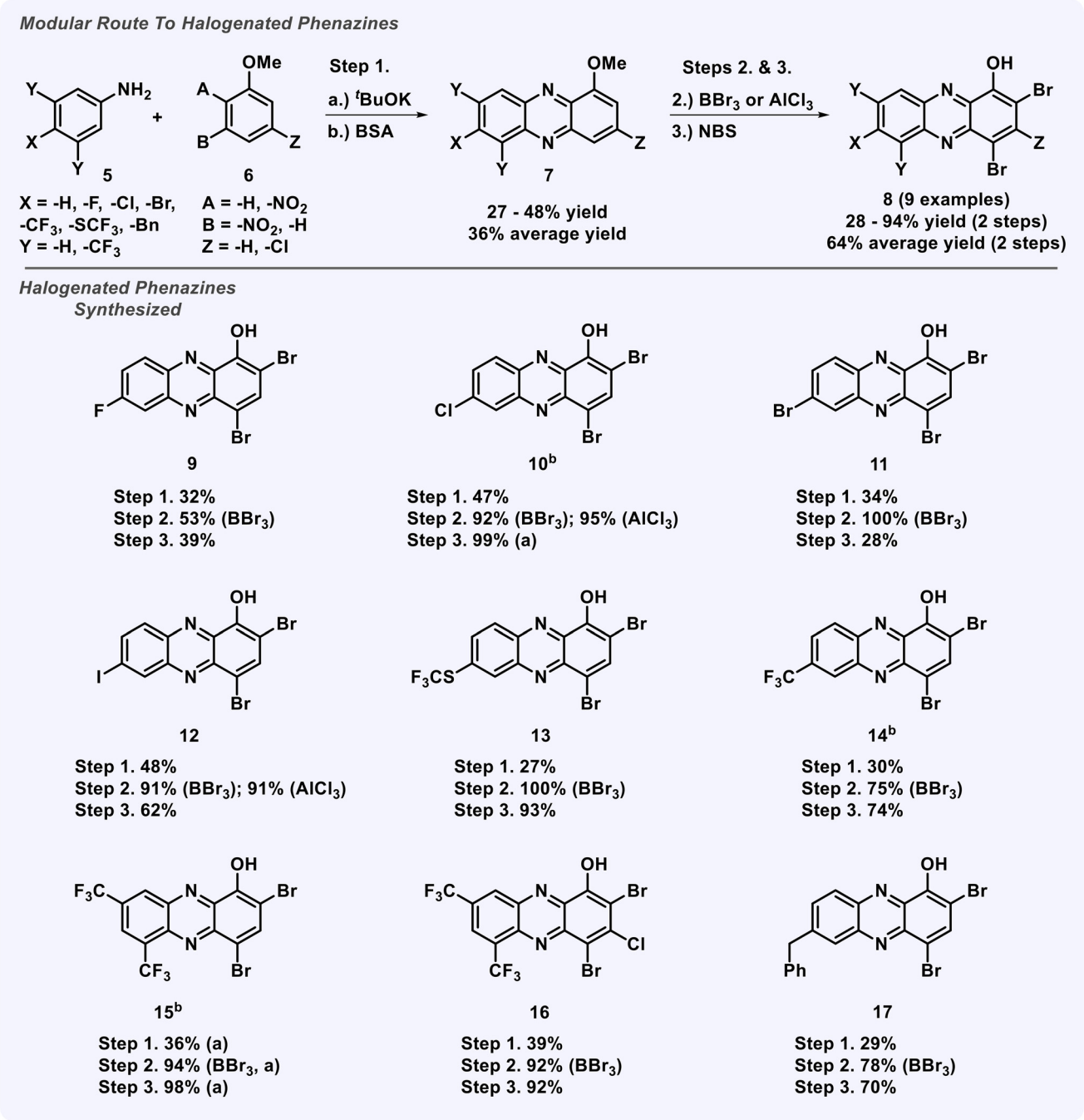


**Scheme 1** Modular synthesis of halogenated phenazines from diverse nitroarene and aniline materials. Notes. (a) Demethylation or bromination yields from previous studies. (b) Previously reported halogenated phenazines.

When evaluated against Gram-negative pathogens, new HPs reported minimal antibacterial activities. With that, HP **15** was found to report moderate to weak antibacterial activities against *A. baumannii* strains (MIC = 12.5–75 μM; ESI Table 2†); however, **15** was inactive against *P. aeruginosa* or *E. coli* strains (MIC > 100 μM).

Following initial MIC assessment, we performed UV-vis spectroscopy experiments to evaluate iron(II)-binding properties of synthesized HP analogues (Fig. 3C; ESI†). In these UV-vis experiments, we observed an elevated absorbance between 550 nm to 650 nm of HP samples following the addition of iron(II) due to the rapid binding between the HP analogues and iron(II) after 1 and 10 minutes. Our findings that HP analogues directly bind iron(II) support the notion that these HPs are able to induce iron starvation in bacteria as their primary mode of action and aligns with previous studies.[53–55,61]

In addition, we have found several HPs to demonstrate good antibacterial activities against *Mycobacterium tuberculosis* (MIC <

Open Access Article. Published on 06 January 2025. Downloaded on 2/6/2026 5:04:38 PM.
This article is licensed under a Creative Commons Attribution-NonCommercial 3.0 Unported Licence.

Table 1 Summary of antibacterial studies (MIC) and cytotoxicity assessment for halogenated phenazines and select antibiotics

| Compound | MRSA 1707 | MRSA 44 | MRSE 35984 | *S. epi* 12228 | VRE 700221 | *E. faecalis* OG1RF | *S. pneumoniae* 6303 | *Mtb* (rep) | *Mtb* (dorm) | HeLa cytotox. ($IC_{50}$) |
|---|---|---|---|---|---|---|---|---|---|---|
| **1 (HP-1)** | 1.17[a] | 1.56 | 1.17[a] | 1.17[a] | 4.69[a] | 18.8[a] | 1.56 | 15.8 | 200 | >100 |
| **9** | 0.30[a] | 0.39 | 0.39 | — | 2.35[a] | 6.25 | 0.39 | — | — | >100 |
| **10** | 0.08[a] | 0.10 | 0.15[a] | 0.10 | 1.56 | 3.13 | 0.20 | — | — | >100 |
| **11** | 0.05 | 0.10 | 0.30[a] | — | 1.17[a] | 3.13 | 0.39 | — | — | >100 |
| **12** | 0.08[a] | 0.05[b] | 0.15[a] | 0.08[a] | 0.78 | — | 0.20 | — | — | >100 |
| **13** | 0.04[a] | 0.05[b] | 0.10 | 0.10 | 0.39 | 0.78 | 0.08[a] | — | — | >100 |
| **14** | 0.05 | 0.05[b] | 0.10 | — | 0.39 | 0.78 | 0.08[a] | — | — | >100 |
| **15** | 0.05[b] | 0.05[b] | 0.08[a] | 0.15[a] | 0.05[b] | 0.20 | 0.08[a] | 3.69 | 1.35 | >100 |
| **16** | 1.17[a] | 0.78 | 0.20 | 1.56 | 3.13 | 4.69[a] | 1.56 | — | — | — |
| **17** | 0.30[a] | 0.20 | 0.15[a] | 0.10 | 0.59[a] | 4.69[a] | 0.78 | — | — | — |
| **Vancomycin** | 0.59[a] | 0.59[a] | 1.17[a] | 1.56 | >100 | 0.78 | 0.39 | — | — | — |
| **Isoniazid** | — | — | — | — | — | — | — | 0.1 | 114.7 | — |
| **Rifamycin** | — | — | — | — | — | — | — | 0.001 | 1.43 | — |

All MIC values against bacterial pathogens and cytotoxicity against HeLa cells are reported in micromolar (μM) concentrations. All biological results were acquired from three or more independent experiments. [a] Midpoint value for 2-fold range in MIC values observed. [b] Lowest concentration tested. "*Mtb* (rep)" refers to replicating *Mtb* CDC1551 bacteria; "*Mtb* (dorm)" refers to dormant *Mtb* CDC1551 bacteria.

2 μM) in previous work.[53] With the antibacterial activity profiles in hand, we were encouraged to investigate HP **15** against both replicating and dormant *Mtb* cultures (Table 1). Although **HP-1** was able to inhibit replicating *Mtb* with an MIC = 15.8 μM, only weak activity was observed against dormant bacilli (MIC = 200 μM). A similar pattern of drug tolerance was reported for the first-line anti-TB drugs isoniazid (INH) and rifampin (RIF), with dormant *Mtb* becoming more than 1000 times more tolerant to these drugs than the replicating bacteria. In contrast, HP **15** exhibited significantly improved potency against replicating *Mtb* (MIC = 3.69 μM) than **HP-1** and, unexpectedly, even better activity against dormant *Mtb* (MIC = 1.35 μM). Additional work is needed to better understand the unique activity HP **15** demonstrates against dormant *Mtb*.

## Mammalian cytotoxicity

Following MIC assessment, eight HPs were evaluated against HeLa cells to determine bacteria-to-mammalian selectivity using 24 hours lactate dehydrogenase assays at 25, 50, and 100 μM test concentrations (Table 1). Similar to previous studies,[52,53] these HPs demonstrated minimal to no cytotoxicity against HeLa cells ($IC_{50}$ > 100 μM). Selectivity indexes (SI) were determined based on relative $IC_{50}$ values against HeLa cells compared to MIC values against *S. aureus* (HeLa [$IC_{50}$]/*S. aureus* [MIC]) to show most HPs demonstrate impressive SI > 300 during these studies.

## Biofilm eradication studies with halogenated phenazines

After determining initial antibacterial activities from MIC and HeLa cell cytotoxicity assays, we evaluated HPs against established MRSA, MRSE, MSSE (methicillin-sensitive *S. epidermidis*), and VRE biofilms using Calgary Biofilm Device (CBD) assays[62,63] (Fig. 4; Table 2). CBD assays are performed in 96-well plates and utilize specialized lids with pegs that are submerged into media (1 peg per microtiter well; see ESI†) to provide a surface for bacteria to attach and form biofilms.[62,63] Biofilm eradication assays have three distinct phases, which include: (1) establishing biofilms on CBD peg surfaces (bacteria in media alone), (2) compound challenge (biofilm-associated CBD pegs are submerged into a 96-well plate containing test compounds in 2-fold serial dilution), and (3) biofilm dispersion and growth (this final phase includes CBD pegs incubated in media alone to facilitate the dispersion of viable planktonic bacteria from biofilms followed by growth to give a final turbid readout; note: biofilms that have been eradicated result in a complete lack of turbidity at the assay end point).

Each of the three phases of our CBD assays were performed under static conditions for 24 hours at 37 °C (experiments require 72-hours total to complete). Biofilm-attached pegs were gently washed with PBS to remove planktonic cells between each of the three phases of the MBEC assay (lid transfer steps). Upon completion of CBD assays, turbidity measurements were taken using a spectrophotometer ($OD_{600}$) to quantify (1) viable biofilms that undergo planktonic dispersion and subsequent bacterial growth (visible turbidity), or (2) eradicated biofilms (no turbidity results from completely eradicated biofilms unable to disperse planktonic bacteria; see Fig. 4B for representative CBD assays against MRSA lab strain & clinical isolate). Following the completion of CBD assays, the minimum biofilm eradication concentration (MBEC) for test compounds is determined as the lowest concentration resulting in complete biofilm killing (no turbidity in microtiter wells). In addition to biofilm killing, CBD assays also provide direct planktonic eradication assessment of test compounds following dilution from the test plate (phase 2) into fresh media and subsequent incubation for 24 hours to determine minimum bactericidal concentrations (CBD). This assay allows

Open Access Article. Published on 06 January 2025. Downloaded on 2/6/2026 5:04:38 PM.
This article is licensed under a Creative Commons Attribution-NonCommercial 3.0 Unported Licence.

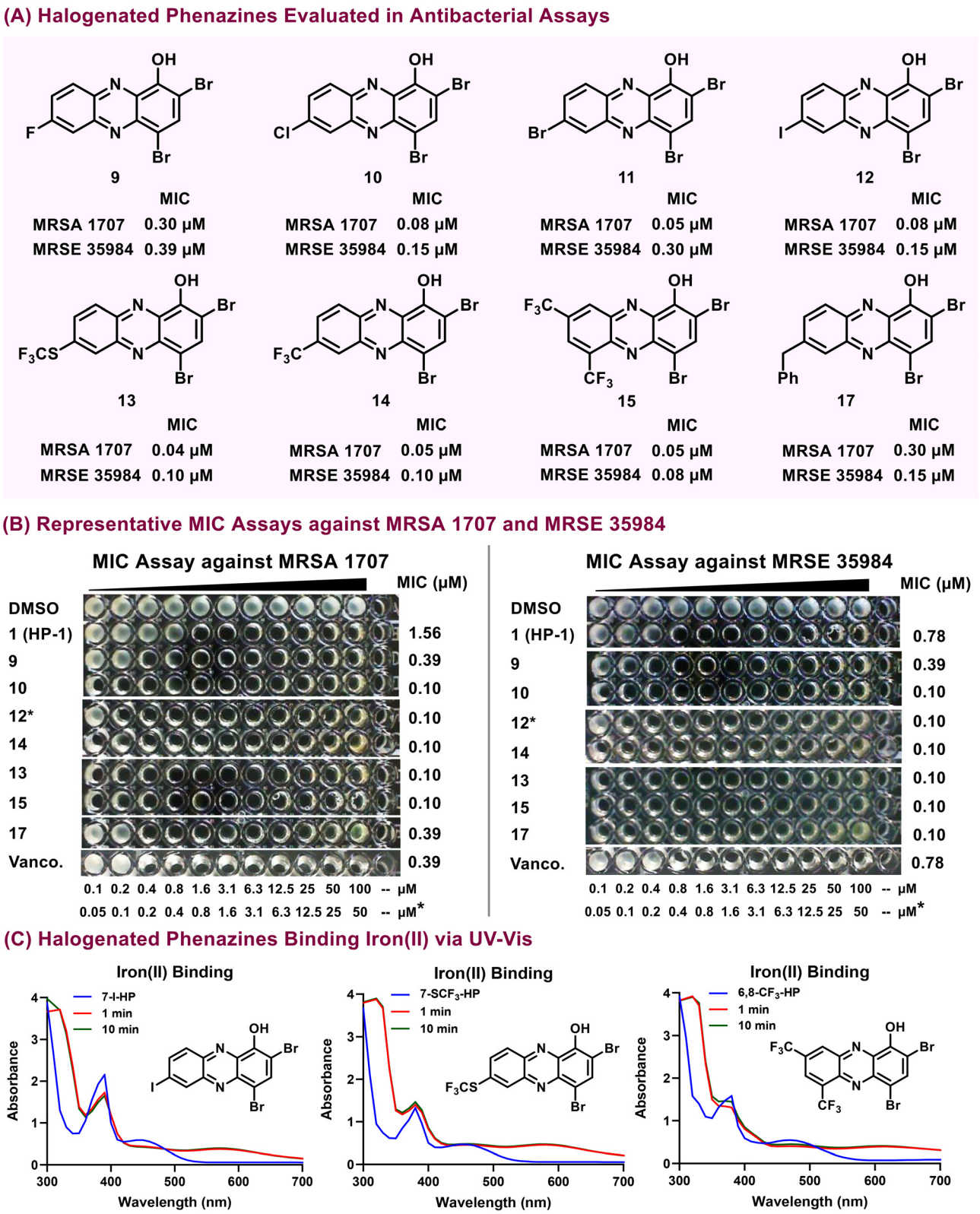


**Fig. 3** (A) Chemical structures and focused antibacterial profiles (against MRSA 1707 & MRSE 35984) for potent halogenated phenazines investigated during these studies. (B) Images of representative MIC assays against MRSA 1707 and MRSE 35984. (C) UV-vis experiments to show select HPs directly binding iron(II).

Open Access Article. Published on 06 January 2025. Downloaded on 2/6/2026 5:04:38 PM.
This article is licensed under a Creative Commons Attribution-NonCommercial 3.0 Unported Licence.

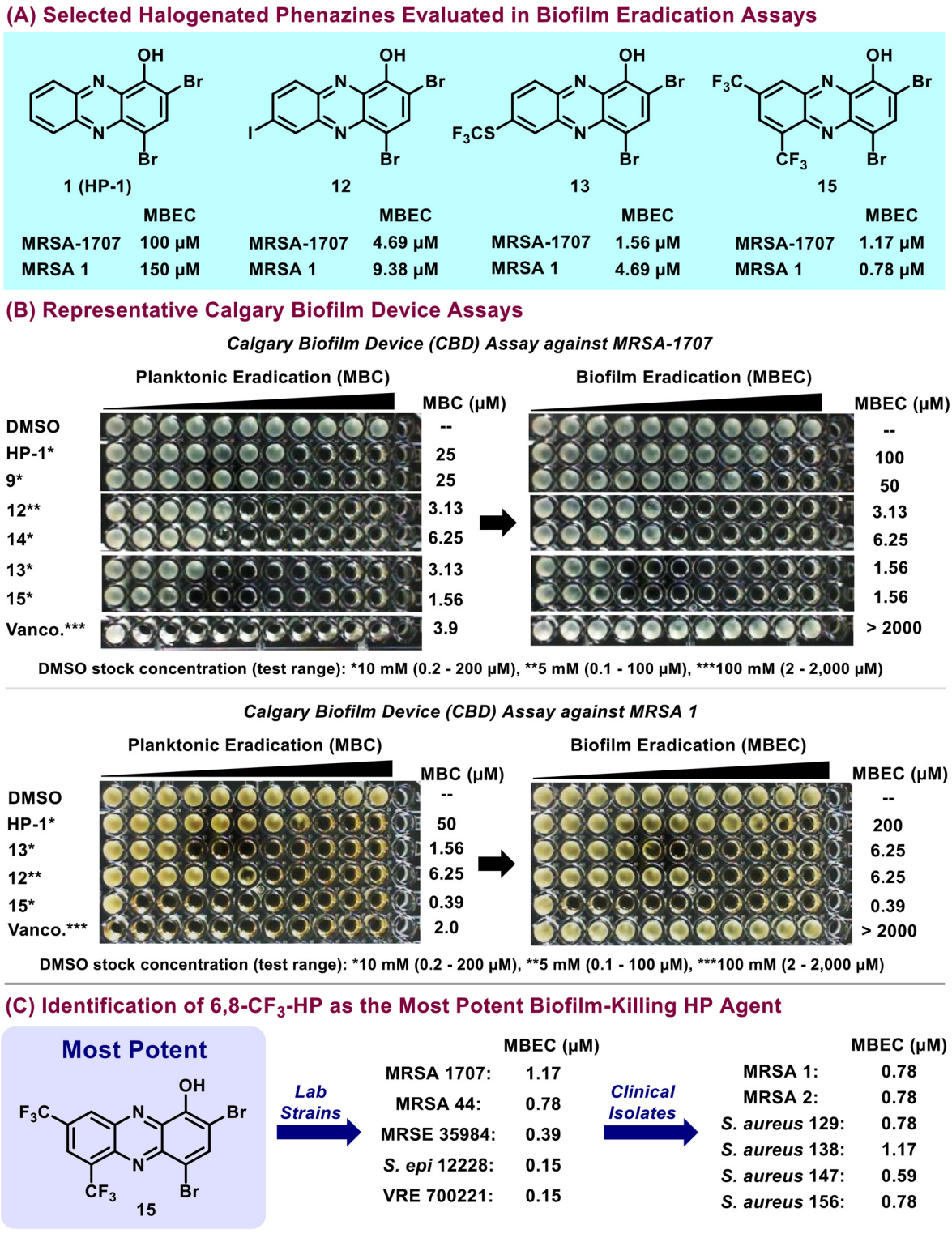


**Fig. 4** (A) Select halogenated phenazine biofilm eradication activities. (B) Representative MBEC images of halogenated phenazines evaluated in Calgary Biofilm Device (CBD) assays. (C) Biofilm eradication profile for HP **15**. Note: *Compounds were tested from 0.2 µM to 200 µM (10 mM DMSO stock solution). **Compounds were tested from 0.1 µM to 100 µM (5 mM DMSO stock solution). ***Compounds were tested from 2 µM to 2000 µM (100 mM DMSO stock solution).

 This journal is © The Royal Society of Chemistry 2025

Open Access Article. Published on 06 January 2025. Downloaded on 2/6/2026 5:04:38 PM.
This article is licensed under a Creative Commons Attribution-NonCommercial 3.0 Unported Licence.

**Table 2** Summary of biofilm eradication activities using the Calgary Biofilm Device assay along with follow-up hemolysis activities for halogenated phenazines and comparator test molecules

| Compound | MRSA 1707 MBC/MBEC | MRSA 44 MBC/MBEC | MRSE 35984 MBC/MBEC | *S. epidermidis* 12228 MBC/MBEC | VRE 700221 MBC/MBEC | % Hemolysis at 200 μM |
|---|---|---|---|---|---|---|
| **1 (HP-1)** | 50[b]/100[b] | 100/100[b] | 50[b]/100 | 25[b]/50[b] | 18.8[a]/9.38[a] | ≤1 |
| **9** | 37.5[a]/37.5[a] | 50/12.5 | 50/75[a] | 3.13/37.5[a] | nd/3.13[b] | 1.6 |
| **10** | 1.17[a]/4.69[a] | 12.5/4.69[a] | 25/50 | — | 1.56[b]/0.59[a] | ≤1 |
| **11** | 4.69[a]/9.38[a] | 9.38[a]/18.8[a] | 12.5/12.5 | — | 18.8[a]/25 | 1.6 |
| **12** | 4.69[a]/4.69[a] | 37.5[a]/18.8[a] | 25/37.5[a] | 1.56[b]/4.69[a] | — | ≤1 |
| **13** | 2.35[a]/1.56 | 3.13[b]/3.13[b] | 3.13/2.35[a] | 1.17[a]/1.17[a] | 0.15[a]/0.10[c] | ≤1 |
| **14**[d] | 4.69[a]/4.69[a] | 4.69[a]/9.38[a] | 12.5/12.5 | 3.75[a]/3.75[a] | 9.38[a]/0.39 | 7.2 |
| **15** | 1.17[a]/1.17[a] | 0.30[a]/0.78[b] | 0.20[c]/0.39[b] | 0.10[c]/0.15[a] | 0.10[c]/0.15[a] | 7.8 |
| **16** | 25[b]/12.5 | — | 1.17[a]/1.17[a] | — | — | — |
| **17** | 9.38[a]/6.25 | — | 12.5/75[a] | 25[b]/18.8[a] | — | ≤1 |
| **QAC-10** | 93.8[a]/93.8[a] | — | 3.13/3.13 | 4.69[a]/6.25 | 3.0[a]/3.0[a] | >99 |
| **EDTA** | >2000/>2000 | — | 1000/>2000 | — | — | ≤1 |
| **TPEN** | 375[a]/>2000 | — | 250/>2000 | — | — | ≤1 |
| **Vancomycin** | 3.9/>2000 | 7.8/>2000 | 3.0[b]/>2000 | — | >200/150 | ≤1 |

All biological results in this table are reported in micromolar (μM) concentrations and were acquired from three or more independent experiments. [a] Midpoint value for experiments that yielded a 2-fold range from CBD assays. [b] Midpoint value for experiments that yielded a 4-fold range from CBD assays. [c] Lowest concentration tested. [d] For HP compound **14**, we previously reported CBD assay values of MBC = 3.13 μM & MBEC = 4.69 μM against MRSE 35984 (see compound 5h in ref. 54). nd = not determined due to an uncharacteristically large range of planktonic killing activities in these assays against VRE 700221.

for the determination of biofilm and planktonic killing dynamics of various small molecules from a single experiment.

During these studies, we evaluated all HPs in CBD assays against MRSA 1707 and MRSE 35984 biofilms to determine MBEC values against these major human pathogens (Table 2). Select HP analogues were also evaluated against MRSA 44, *S. epidermidis* 12228, and VRE 700221 biofilms. From our CBD experiments, we found biofilm-killing profiles analogous to the antibacterial properties as each 6-, 7-, or 8-substituted HP demonstrated significantly improved biofilm eradication activities compared to **HP-1**. 7-Fluoro-HP **9** (MBEC = 37.5 μM) demonstrated improved biofilm eradication against MRSA 1707 biofilms when compared to parent **HP-1**; however, HP **9** was found to be 4- to 8-fold less potent than 7-chloro-HP **10**, 7-bromo-HP **11**, 7-iodo-HP **12** (Fig. 4), or 7-trifluoromethyl-HP **14** as these HPs demonstrated potent activities (MBEC = 4.69–9.38 μM) in Calgary Biofilm Device assays. HP **17** (7-benzy-HP; MBEC = 6.25 μM) also demonstrated potent biofilm eradication activities against MRSA 1707 biofilms. Impressively, 7-$SCF_3$-HP **13** demonstrated highly potent biofilm-killing activities in CBD assays against MRSA 1707 (MBEC = 1.56 μM, Fig. 4), MRSA 44 (MBEC = 3.13 μM), MRSE 35984 (MBEC = 2.35 μM), *S. epidermidis* 12228 (MBEC = 1.17 μM), and VRE 70021 (MBEC = 0.10 μM).

We were very encouraged to find 6,8-ditrifluoromethyl-HP **15** eradicates bacterial biofilms with incredible potency against the Gram-positive pathogens in our panel (MRSA 1707, MBEC = 1.17 μM; MRSA 44, MBEC = 0.78 μM; MRSE 35984, MBEC = 0.39 μM; *S. epidermidis* 12228, MBEC = 0.15 μM; VRE 700221, MBEC = 0.15 μM; Fig. 4 and Table 2). HP **15** is the most potent biofilm eradicating agent we have reported to date. 3-Chloro-6,8-ditrifluoromethyl-HP (**16**; MBEC = 12.5 μM) showed a 4- to 11-fold reduction in biofilm-killing properties against MRSE 35984 and MRSA 1707 biofilms, respectively, when compared to 6,8-ditrifluoromethyl-HP **15**.

In addition to examining HPs for their biofilm eradication properties, we evaluated a focused series of comparator agents, including vancomycin – a frontline antibiotic used to treat MRSA infections (Table 2). We evaluated QAC-10 which is a known quaternary ammonium cation agent that has demonstrated biofilm killing properties through a membrane-lysis mode of action.[64] When tested alongside 6,8-ditrifluoromethyl-HP **15**, QAC-10 demonstrated an 8- to 80-fold reduction in biofilm-killing potency reporting MBEC values of 93.8 μM against MRSA 1707, 3.13 μM against MRSE 35984, 6.25 μM against *S. epidermidis* 12228, and 3.0 μM against VRE 700221 biofilms. Since HP biofilm-eradicating agents operate through an iron starvation mode of action, we evaluated metal-chelating agents EDTA (general chelator) and TPEN (cell-permeable chelator) as comparators; however, neither of these compounds were able to eradicate MRSA or MRSE biofilms (MBEC > 2000 μM). Vancomycin was evaluated in CBD assays against MRSA, MRSE and VRE biofilms. Against MRSA and MRSE, we found vancomycin to report potent planktonic killing activities (MBC = 3.0–7.8 μM) while their biofilm counterparts were completely tolerant to this antibiotic (MBEC > 2000 μM). Interestingly, we did observe vancomycin to eradicate VRE 700221 biofilms at high concentrations (MBEC = 150 μM), which is attributed to a less robust biofilm under these assay conditions.

We then performed hemolysis assays to determine if this series of HPs demonstrates membrane-lysis activities following initial biofilm eradication studies. Hemolysis assays are an important secondary experiment when evaluating biofilm-killing profiles of small molecules as general membrane lysis is an effective way to eradicate established biofilms (*i.e.*, quaternary ammonium cations such as QAC-10 induce >99%

Open Access Article. Published on 06 January 2025. Downloaded on 2/6/2026 5:04:38 PM.
This article is licensed under a Creative Commons Attribution-NonCommercial 3.0 Unported Licence.

hemolysis of red blood cells at 200 μM and kill biofilms; Table 2). During these studies, eight HPs were evaluated against red blood cells at 200 μM to give <8% hemolysis activity at this high test concentration demonstrating that these HPs do not operate through a membrane lysis mechanism.

Following initial biofilm eradication assessment, **HP-1**, 6,8-ditrifluoromethyl-HP **15**, 7-$SCF_3$-HP **13**, 7-iodo-HP **12**, and vancomycin were evaluated against a panel of six MRSA clinical isolates in CBD assays (Table 3). Against MRSA isolates, **HP-1** demonstrated moderate to low biofilm-killing activities with MBECs = 150–>200 μM while 7-$SCF_3$-HP **13** and 7-iodo-HP **12** reported good to excellent activities (MBEC values = 4.69–25 μM). 6,8-ditrifluoromethyl-HP **15** demonstrated incredible biofilm-killing properties against MRSA clinical isolates with MBEC values = 0.59–1.17 μM. In addition, vancomycin was used as a comparator against this panel of MRSA clinical isolates. Despite vancomycin's potent activity against planktonic cells (MBC = 3.0–7.8 μM; Table 3) in CBD assays, the drug of last resort for MRSA infections was unable to eradicate MRSA biofilms at the highest concentrations tested (MBEC values > 2000 μM against all isolates).

## Confocal microscopy reveals matrix loss with HP treatment

To visualize the MRSA biofilm matrix modulation of 6,8-ditrifluoromethyl-HP **15** we utilized confocal *z*-stack imaging with USA300 *S. aureus* carrying pCM29_GFP. This plasmid allows for the constitutive expression of green fluorescent protein (GFP) and imaging of the biofilm cell population. To visualize the associated biofilm matrix, we stained the biofilms before imaging with concanavalin A lectin conjugated with Texas Red. This combination allows for visualization of both the bacteria and the matrix polysaccharides of the *S. aureus* biofilms.

We found that treatment of a pre-formed MRSA biofilm with both parent **HP-1** (**1**) and 6,8-ditrifluoromethyl-HP **15** at 25 μM could reduce the biofilm height, although HP **15** was far superior at this concentration (Fig. 5). Specifically, the

**Table 3** Summary of Calgary Biofilm Device assay results for select halogenated phenazines and vancomycin against MRSA clinical isolates

| Compound | MRSA 1 MBC/MBEC | MRSA 2 MBC/MBEC | *S. aureus* 129 MBC/MBEC | *S. aureus* 138 MBC/MBEC | *S. aureus* 147 MBC/MBEC | *S. aureus* 156 MBC/MBEC |
|---|---|---|---|---|---|---|
| **1 (HP-1)** | 37.5[a]/150[a] | 37.5[a]/≥200 | 75[a]/>200 | 50/200 | 50/≥200 | 50/≥200 |
| **12** | 6.25/9.38[a] | 6.25/18.8[a] | 12.5[b]/18.8[a] | 12.5/18.8[a] | 9.38[a]/9.38[a] | 9.38[a]/12.5 |
| **13** | 2.35[a]/4.69[a] | 4.69[a]/18.8[a] | 2.35[a]/9.38[a] | 12.5/25 | 6.25/9.38[a] | 3.13/6.25 |
| **15** | 0.59[a]/0.78[b] | 0.59[a]/0.78[b] | 0.59[a]/0.78 | 1.56/1.17[a] | 0.78[b]/0.59[a] | 0.78/0.78[b] |
| **Vancomycin** | 3.0[a]/>2000 | 5.9[a]/>2000 | 5.9[a]/>2000 | 7.8/>2000 | 5.9[a]/>2000 | 7.8/>2000 |

All biological results are reported in micromolar (μM) concentrations and were acquired from three or more independent experiments. [a] Midpoint value for experiments that yielded a 2-fold range from CBD assays. [b] Midpoint value for experiments that yielded a 4-fold range from CBD assays.

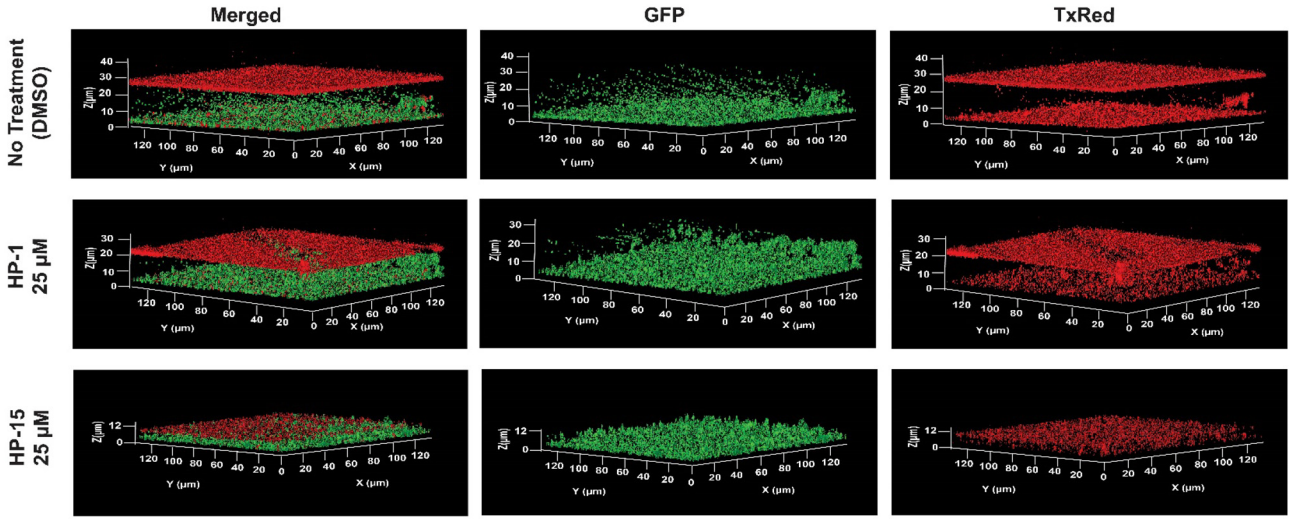


**Fig. 5** Confocal microscopy images of MRSA biofilms untreated or treated with select HP analogues. The figures show the 3-D rendering of confocal *z*-stack imaging of biofilms grown with GFP expressing *S. aureus* and stained with Texas Red conjugated concanavalin A. The top three images show MRSA biofilms with no compound (DMSO Control), the middle and bottom images are those treated with 25 μM of **HP-1** and 6,8-ditrifluoromethyl-HP **15**, respectively. All imaging was done with $n = 3$ replicates with representative images shown.

Open Access Article. Published on 06 January 2025. Downloaded on 2/6/2026 5:04:38 PM.
This article is licensed under a Creative Commons Attribution-NonCommercial 3.0 Unported Licence.

untreated biofilms had a height of ~30 μm with a dense layer of polysaccharide encasing the bacterial cells. With **HP-1** treatment, this height decreased to ~20 μm and the polysaccharide matrix was much less dense than the untreated biofilms. Following treatment with 6,8-ditrifluoromethyl-HP **15**, there was a drastic reduction in biofilm height (~10 μm height remained) and the polysaccharide matrix on top of the biofilm was largely removed. The images in Fig. 5 validate the increased potency of the optimized 6,8-ditrifluoromethyl-HP **15** compound over parent **HP-1**.

## Conclusions

In conclusion, we have developed a modular synthetic route to access HPs utilizing a reaction sequence that starts from nitroarene and aniline materials to yield diverse 1-methoxyphenazines. Several new HPs demonstrated highly potent antibacterial (MIC ≤ 0.39 μM) and biofilm-eradicating properties (MBEC < 10 μM) with 6,8-ditrifluoromethyl-HP **15** demonstrating the most potent biofilm-killing properties (MBEC = 0.15–1.17 μM) against Gram-positive pathogens, including MRSA clinical isolates. Using confocal microscopy, 6,8-ditrifluoromethyl-HP **15** was shown to induce significant polysaccharide loss of MRSA biofilms. In addition, HP **15** demonstrated increased antibacterial activity against dormant *Mtb* cultures (MIC = 1.35 μM) when compared to replicating *Mtb* (MIC = 3.69 μM). Overall, this modular synthesis enabled rapid access to new halogenated phenazines to further explore their unique antibacterial and biofilm-killing properties.

## Experimental

### General information

All synthetic reactions were carried out under an inert atmosphere of argon unless otherwise specified. All reagents for chemical synthesis were purchased from commercial sources and used without further purification. Reagents were purchased at ≥95% purity and commercially available controls were used in our biological investigations without further purification. Analytical thin layer chromatography (TLC) was performed using 250 μm Silica Gel 60 F254 pre-coated plates (EMD Chemicals Inc.). Flash column chromatography was performed using 230–400 Mesh 60 Å Silica Gel from Sorbent Technologies. All melting points were obtained, uncorrected, using a Mel-Temp capillary melting point apparatus from Laboratory Services, Inc.

NMR experiments were recorded on the following instruments: Bruker Avance III HD and Avance Neo spectrometers (600 MHz and 400 MHz for $^1$H NMR; 151 MHz and 101 MHz for $^{13}$C NMR), and Agilent Systems VNMRS spectrometer (500 MHz for $^1$H NMR; 126 MHz for $^{13}$C NMR). All spectra are presented using MestReNova (Mnova) software and are displayed without the use of the signal suppression function. Spectra were obtained in the following solvents (reference peaks also included for $^1$H and $^{13}$C NMRs): $CDCl_3$ ($^1$H NMR, 7.26 ppm; $^{13}$C NMR, 77.23 ppm) and DMSO-$d_6$ ($^1$H NMR: 2.50 ppm, $^{13}$C NMR, 39.52 ppm). All NMR experiments were performed at room temperature. Chemical shift values ($\delta$) are reported in parts per million (ppm) for all $^1$H NMR and $^{13}$C NMR spectra. $^1$H NMR multiplicities are reported as: s = singlet, br. s = broad singlet, d = doublet, q = quartet, m = multiplet. High-Resolution Mass Spectrometry (HRMS) were obtained for new compounds from the Chemistry Department at the University of Florida.

Bacterial strains used during these investigations include: methicillin-resistant *Staphylococcus aureus* (ATCC BAA-1707 and ATCC BAA-44; Clinical Isolates from Shands Hospital in Gainesville, FL: MRSA 1, MRSA 2, *S. aureus* 129, *S. aureus* 138, *S. aureus* 147, & *S. aureus* 156), methicillin-sensitive *Staphylococcus epidermidis* (ATCC 12228), methicillin-resistant *Staphylococcus epidermidis* (MRSE, ATCC 35984), *Enterococcus faecalis* (ATCC OG1RF), vancomycin-resistant *Enterococcus* (VRE, ATCC 700221), *Streptococcus pneumonia* (ATCC 6303), *Mtb*-lux (strain CDC1551 transformed with pMV306hsp+LuxG13), multidrug-resistant (MDR) *Acinetobacter baumannii* (ATCC 1794, ATCC 19606, & ATCC 17978), *Pseudomonas aeruginosa* (ATCC PA01), and *Escherichia coli* (Clinical Isolate UAEC-1). *S. aureus* strain AH3669 constitutively expressing GFP was used for confocal microscopy experiments.

All compounds were stored as dimethyl sulfoxide (DMSO) stocks at room temperature in the absence of light. To ensure compound integrity of DMSO stock solutions of our test compounds, we did not subject them to freeze–thaw cycles.

### Minimum inhibitory concentration (MIC) susceptibility assay against ESKAPE pathogens

The minimum inhibitory concentration (MIC) for each test compound was determined by the broth microdilution method as recommended by the Clinical and Laboratory Standards Institute (CLSI).[65] In a 96-well plate, two-fold serial dilutions of each test compound were made in a final volume of 100 μL of broth (Lysogeny Broth or LB for *S. aureus*, *S. epidermidis* MRSE 35984, *S. pneumonia*, *A. baumannii*, *P. aeruginosa* and *E. coli*; TSBG was required for *S. epidermidis* 12228 as this strain for optimal growth for MIC assays; Brain Heart Infusion for *E. faecium* and *E. faecalis*). Each microtiter well was inoculated with ~$10^5$ bacterial cells at the initial time of incubation, prepared from a fresh log phase culture ($OD_{600}$ 0.5–1.0). The MIC was defined as the lowest concentration of a compound that completely inhibits bacterial growth after incubating for 16 hours at 37 °C (MIC values were determined by visual inspection of turbidity and spectrophotometric readings at $OD_{600}$ to show ≥90% bacterial growth inhibition compared to DMSO vehicle control). The concentration range tested during this study was 0.1 to 100 μM. DMSO served as our vehicle and negative control in each microdilution MIC assay. DMSO was serially diluted with a top concentration of 1% v/v. All compounds were tested in three or more independent experiments.

Open Access Article. Published on 06 January 2025. Downloaded on 2/6/2026 5:04:38 PM.
This article is licensed under a Creative Commons Attribution-NonCommercial 3.0 Unported Licence.

### Minimum inhibitory concentrations against replicating *Mtb*

*Mtb*-lux (strain CDC1551 transformed with pMV306hsp+LuxG13) were grown aerobically in Middlebrook 7H9 (supplemented with glycerol, 0.05% Tween 80, 10% oleic acid-albumin-dextrose-catalase (OADC), 50 μg $mL^{-1}$ Kanamycin) until log phase ($OD_{600}$ 0.8–1.0). After diluting to $OD_{600}$ 0.02, 15 μL of *Mtb*-lux was added into each well of 384-well plates containing the drugs serially diluted (1 : 2) (final volume per well = 30 μL; final *Mtb* $OD_{600}$ per well = 0.01). Luminescence readouts were taken using the Synergy H4 plate reader (BioTek) after 4–5 days of incubation at 37 °C, 5% $CO_2$.[66] Isoniazid and rifampicin curves were included against replicating *Mtb* in complete Dubos medium for comparison of MIC values.[66] MIC values against *Mtb* were defined as the concentration required to give 99% growth inhibition from on dose–response curves generated in GraphPad Prism 10 using the Gompertz model based on positive (rifamycin at 15 μM served as 100% growth inhibition) and negative (1% DMSO) controls. Experimental results were obtained from duplicates in at least two independent assays.

### Minimum inhibitory concentrations against dormant *Mtb*

To determine MICs against drug-tolerant non-replicating dormant *Mtb*, we utilized our previously reported multi-stress dormancy model.[66,67] Briefly, replicating *Mtb*-lux were grown aerobically in Middlebrook 7H9 as described above. After reaching log phase, the culture was pre-adapted in Complete Dubos Medium (CDM) supplemented with 10% ADS for 48 hours. Then, the cells were resuspended in Multiple Stress Dormancy Media (pH = 5.0) and kept for 9 days under hypoxia (37 °C, 5% $O_2$, 10% $CO_2$). At the day 9, the dormant *Mtb* was exposed to serially diluted test compounds and after 48 hours of treatment, the luminescence readouts were taken using the Synergy H4 plate reader (BioTek). Isoniazid and rifampicin curves were included against dormant *Mtb* in complete Dubos medium for comparison of MIC values.[66] MIC values against *Mtb* were defined as the concentration required to give 99% growth inhibition from on dose–response curves generated in GraphPad Prism 10 using the Gompertz model based on positive (rifamycin at 15 μM served as 100% growth inhibition) and negative (1% DMSO) controls. Experimental results were obtained from duplicates in at least two independent assays.

### LDH release assay for HeLa cytotoxicity assessment

HeLa cytotoxicity was assessed using the LDH release assay described by CytoTox96 (Promega G1780). HeLa cells were grown in Dulbecco's Modified Eagle Medium (DMEM; Gibco) supplemented with 10% Fetal Bovine Serum (FBS) at 37 °C with 5% $CO_2$. When the HeLa cultures exhibited 70–80% confluence, halogenated phenazines were then diluted by DMEM (10% FBS) at concentrations of 25, 50 and 100 μM and added to HeLa cells. Triton X-100 (at 2% v/v) was used as the positive control for maximum lactate dehydrogenate (LDH) activity in this assay (*i.e.*, complete cell death) while "medium only" lanes served as negative control lanes (*i.e.*, no cell death). DMSO was used as our vehicle control. HeLa cells were treated with compounds for 24 hours and then 50 μL of the supernatant was transferred into a fresh 96-well plate where 50 μL of the reaction mixture was added to the 96-well plate and incubated at room temperature for 30 minutes. Finally, Stop Solution (50 μL) was added to the incubating plates and the absorbance was measured at 490 nm. Results are from three independent experiments.

### Calgary biofilm device (CBD) assays

Biofilm eradication experiments were performed using the Calgary Biofilm Device to determine MBC/MBEC values for various compounds of interest (Innovotech, product code: 19111). The Calgary device (96-well plate with lid containing pegs to establish biofilms) was inoculated with 125 μL of a mid-log phase culture diluted 1000-fold in tryptic soy broth with 0.5% glucose (TSBG) to establish bacterial biofilms after incubation at 37 °C for 24 hours. The lid of the Calgary device was then removed, gently washed and transferred to a new 96-well plate containing 2-fold serial dilutions of the test compounds in media (the "challenge plate"). The total volume of media with compound in each well in the challenge plate is 150 μL. The Calgary device was then incubated at 37 °C for 24 hours. The lid was then removed from the challenge plate and MBC/MBEC values were determined using different experimental pathways. To determine MBC values, 20 μL of the challenge plate was transferred into a fresh 96-well plate containing 180 μL TSBG and incubated overnight at 37 °C. The MBC values were determined as the test concentration of compound that resulted in a complete lack of visible bacterial growth (*i.e.*, turbidity). For determination of MBEC values, the Calgary device lid (with attached pegs/treated biofilms) was transferred to a new 96-well plate containing 150 μL of fresh TSBG media in each well and incubated for 24 hours at 37 °C to allow viable biofilms to grow and disperse resulting in turbidity after the incubation period. MBEC values were determined as the lowest test concentration that resulted in microtiter wells with no turbidity as a result of complete biofilm eradication. Notes: All data were obtained from a minimum of three independent experiments. MBC & MBEC values were determined as the lowest test concentration required to demonstrate ≥90% reduction in turbidity compared to the DMSO control as determined with the use of a spectrophotometer based on $OD_{600}$ values (with background subtracted; see ESI†).

### Hemolysis assay with red blood cells

Freshly drawn human red blood cells (hRBC with ethylenediaminetetraacetic acid, EDTA, as an anticoagulant) were washed with Tris-buffered saline (0.01 M Tris-base, 0.155 M sodium chloride, pH 7.2) and centrifuged for 5 minutes at 3500 rpm. The washing was repeated three times with the buffer. In a 96-well plate, test compounds were added to the buffer from DMSO stocks. Then 2% hRBCs (50 μL) in buffer were added to test compounds to give a final concentration of 200 μM. The plate was then incubated for 1 hour at 37 °C. After incubation, the plate was then centrifuged for 5 minutes at 3500 rpm. Then, 80 μL of the supernatant was transferred to another

 This journal is © The Royal Society of Chemistry 2025

Open Access Article. Published on 06 January 2025. Downloaded on 2/6/2026 5:04:38 PM.
This article is licensed under a Creative Commons Attribution-NonCommercial 3.0 Unported Licence.

96-well plate and the optical density (OD) was read at 405 nm. DMSO served as our negative control (0% hemolysis) while Triton X served as our positive control (100% hemolysis). The percent hemolysis was calculated as ($OD_{405}$ of the compound − $OD_{405}$ DMSO)/($OD_{405}$ Triton X − $OD_{405}$ buffer) from three independent experiments.

### Confocal microscope images with *Staphylococcus aureus* biofilms

*Staphylococcus aureus* strain AH3669 (USA300-0114 MRSA; pCM29_GFP)[68] constitutively expressing GFP were grown overnight at 37 °C at 220 rpm in tryptic soy broth (TSB) with 10 μg $mL^{-1}$ of chloramphenicol. The resulting cultures were used to seed biofilms at an $OD_{600}$ = 0.5 in Biofilm Media (TSB, 0.5% Glucose) at a volume of 1 mL. Biofilms were seeded in 35 mm Matsunami glass bottom culture dishes (VWR) with glass thickness of #1.5 (0.16–0.19 mm). The edges of the dish were sealed with parafilm, and the biofilms were grown for 24 hours 37 °C under static conditions. After 24 hours of growth, the supernatant was carefully aspirated so as not to disturb bacteria adhered to the dish. The halogenated phenazine compounds were diluted in Mueller Hinton 2 broth (MHBII) from the stock concentration (10 mM) to the appropriate concentration in triplicate. A DMSO control was prepared in triplicate containing an equivalent volume to that of the highest concentration of halogenated phenazine. The dilutions and controls were added to the biofilms, the edges of the dishes were sealed with parafilm, and the biofilms were returned to the 37 °C static bacterial incubator for 24-hour incubation with the treatment. Following treatment, the supernatant was removed, and the biofilms were washed with 1 mL of phosphate buffered saline (PBS). The biofilm polysaccharide matrix material was stained with 1 mL of the 100 μg $mL^{-1}$ Texas Red conjugated Concanavalin A (Invitrogen) in 0.1 M Sodium Bicarbonate for 5 minutes in the dark on a gel rocker. The dye was aspirated, and the samples were washed with 1 mL of PBS to remove residual dye. *Z*-stack images were taken with Zeiss LSM 710 confocal microscope using the 63× oil objective with 488 nm and 543 nm laser channels.

### UV-vis spectroscopy experiments

In a 1.5 mL cuvette were added 970 μL of DMSO and 30 μL of test compound (as a 10 mM DMSO stock solution). In a separate cuvette, 955 μL of DMSO, 30 μL of test compound (10 mM DMSO stock), and 15 μL of ammonium iron(II) sulfate hexahydrate were added (10 mM water solution) and thoroughly mixed. Then, spectral scanning was performed from 300 to 700 nm in 10 nm increments after 1 and 10 minutes. Note: All iron salt solutions were freshly made and added to the cuvette immediately.

## Abbreviations

| | |
|---|---|
| $AlCl_3$ | Aluminium(III) chloride |
| $BBr_3$ | Boron tribromide |
| BHI | Brain Heart Infusion (broth) |
| Bn | Benzyl |
| BSA | *N*,*O*-Bis(trimethylsilyl)acetamide |
| $^t$BuOK | Potassium *tert*-butoxide |
| °C | Degrees celsius |
| CBD | Calgary Biofilm Device |
| CDM | Complete Dubos Medium |
| CF | Cystic fibrosis |
| cytotox. | Cytotoxicity |
| DMEM | Dulbecco's Modified Eagle Medium |
| DMSO | Dimethyl sulfoxide |
| EDTA | Ethylenediaminetetraacetic acid |
| FBS | Fetal Bovine Serum |
| GFP | Green fluorescent protein |
| equiv. | Equivalents |
| HP | Halogenated phenazine |
| HRMS | High resolution mass spectroscopy |
| HSQC | Heteronuclear Single Quantum Coherence |
| INH | Isoniazid |
| LB | Luria–Bertani (broth) |
| LDH | Lactate dehydrogenase |
| M | Molar |
| MBC | Minimum bactericidal concentration |
| MBEC | Minimum biofilm eradication concentration |
| MDR | Multidrug-resistant |
| Me | Methyl |
| MeOH | Methanol |
| mg | Milligram(s) |
| MH | Mueller Hinton (broth) |
| mL | Milliliters |
| mM | Millimolar |
| MIC | Minimum inhibitory concentration |
| μm | Micrometer |
| μM | Micromolar |
| μg | Microgram |
| min | Minute(s) |
| MRSA | Methicillin-resistant *Staphylococcus aureus* |
| MRSE | Methicillin-resistant *Staphylococcus epidermidis* |
| MSSE | Methicillin-sensitive *Staphylococcus epidermidis* |
| *Mtb* | *Mycobacterium tuberculosis* |
| NaCl | Sodium chloride |
| NBS | *N*-Bromosuccinimide |
| nM | Nanomolar |
| nm | Nanometer |
| NMR | Nuclear magnetic resonance (spectroscopy) |
| OADC | Oleic acid-albumin-dextrose-catalase |
| OD | Optical density |
| PBS | Phosphate-buffered silane |
| QAC-10 | Quaternary ammonium cation-10 |
| RBCs | (Human) red blood cells |
| RIF | Rifampicin |
| rpm | Revolutions per minute |
| rt | Room temperature |
| *S. epi* | *Staphylococcus epidermidis* |
| SAR | Structure–activity relationship |
| SI | Selectivity index |
| Supp. | Supplemental |

Open Access Article. Published on 06 January 2025. Downloaded on 2/6/2026 5:04:38 PM.
This article is licensed under a Creative Commons Attribution-NonCommercial 3.0 Unported Licence.

| | |
|---|---|
| TLC | Thin-layer chromatography |
| TPEN | *N*,*N*,*N*′,*N*′-Tetrakis(2-pyridinylmethyl)-1,2-ethanediamine |
| TSB | Tryptic soy broth |
| TSBG | Tryptic soy broth with 0.5% glucose |
| μL | Microliters |
| TxRed | Texas Red (fluorescent dye) |
| VRE | Vancomycin-resistant *Enterococcus faecium* |
| v/v | Volume per volume |

## Author contributions

Q. G. synthesized HPs, evaluated HPs (MIC assays, MBEC assays, iron(II)-binding experiments using UV-vis), and wrote the initial draft of this manuscript. H. Y. synthesized HPs and evaluated HPs (MIC and MBEC assays). J. S. performed confocal imaging experiments with *S. aureus* biofilms. P. C. B. H. evaluated HPs to determine activity profiles against replicating and dormant *Mtb*. K. L. evaluated HPs (MIC and MBEC assays). D. B. synthesized a few HPs and evaluated HPs (MIC and MBEC assays). S. M. evaluated HPs in MIC and MBEC assays. S. J. performed cytotoxicity assessments of HPs against HeLa cells. K. R. directed *Mtb* studies and drafted text describing these experiments. R. M. F. directed confocal imaging experiments and drafted manuscript text pertaining to these experiments. R. H. directed chemical synthesis, evaluation of HPs, coordinated research activities, and finalized writing this manuscript with the input of select authors. All authors have reviewed the data, agree with the findings, and approve the final manuscript.

## Data availability

The data underlying this study are available in the published article and its ESI.† The data contained in the manuscript include: synthesis results (Scheme 1), MIC & MBEC results (Tables 1–3 & Fig. 3–4), confocal biofilm images (Fig. 5). The contents contained in the ESI† include: supporting figures, characterization data for newly synthesized (with tabulated $^{1}$H & $^{13}$C NMR data, HRMS, melting points for solids, and NMR spectra), UV-vis spectroscopy results for iron(II) binding, microbiological assay results, cytotoxicity assay results, and HPLC traces with purity analysis for HPs synthesized and evaluated during these studies.

## Conflicts of interest

There are no conflicts of interest to declare.

## Acknowledgements

We would like to thank the University of Georgia, the University of Florida, and the National Institute of General Medical Sciences of the National Institutes of Health (R35GM153272 to R. W. H.). This work was partially supported by the National Institutes of Health R00AI163295 to R. M. F. D.B. was supported by the NIH/NIGMS T32GM136583 "Chemistry-Biology Interface Training Program" at the University of Florida. We are very grateful for Dr Alexander Horswill from University of Colorado providing us with the *S. aureus* strain AH3669 constitutively expressing GFP. High resolution mass spectra were obtained for novel synthesized compounds from the University of Florida's Mass Spectrometry Research and Education Center and supported by NIH S10 OD021758-01A1. We thank Eli Levit for helpful discussions related to NMR data during the preparation of this manuscript.

## References

1 W. R. Miller and C. A. Arias, ESKAPE Pathogens: Antimicrobial Resistance, Epidemiology, Clinical Impact and Therapeutics, *Nat. Rev. Microbiol.*, 2024, **22**, 598–616.
2 O. Ciofu, C. Moser, P. Ø. Jensen and N. Høiby, Tolerance and Resistance of Microbial Biofilms, *Nat. Rev. Microbiol.*, 2022, **20**, 621–635.
3 Y. Abouelhassan, A. T. Garrison, H. Yang, A. Chávez-Riveros, G. M. Burch and R. W. Huigens III, Recent Progress in Natural-Product-Inspired Programs Aimed to Address Antibiotic Resistance and Tolerance, *J. Med. Chem.*, 2019, **62**, 7618–7642.
4 E. M. Darby, E. Trampari, P. Siasat, M. S. Gaya, I. Alav, M. A. Webber and J. M. A. Blair, Molecular Mechanisms of Antibiotic Resistance Revisited, *Nat. Rev. Microbiol.*, 2023, **21**, 280–295.
5 J. M. Munita and C. A. Arias, Mechanisms of Antibiotic Resistance, *Microbiol. Spectrum*, 2016, **4**, VMBF-0016-2015.
6 G. D. Wright, Molecular Mechanisms of Antibiotic Resistance, *Chem. Commun.*, 2011, **47**, 4055–4061.
7 A. A. Bridges, J. A. Prentice, N. S. Wingreen and B. L. Bassler, Signal Transduction Network Principles Underlying Bacterial Collective Behaviors, *Annu. Rev. Microbiol.*, 2022, **76**, 235–257.
8 K. Lewis, Persister Cells: Molecular Mechanism Related to Antibiotic Tolerance, *Handb. Exp. Pharmacol.*, 2012, **211**, 121–133.
9 K. Schilcher and A. R. Horswill, Staphylococcal Biofilm Development: Structure, Regulation, and Treatment Strategies, *Microbiol. Mol. Biol. Rev.*, 2020, **84**, e00026–e00019.
10 H. Niu, J. Gu and Y. Zhang, Bacterial Persisters: Molecular Mechanisms and Therapeutic Development, *Signal Transduction Targeted Ther.*, 2024, **9**, 174.
11 J. Yan and B. L. Bassler, Surviving as a Community: Antibiotic Tolerance and Persistence in Bacterial Biofilms, *Cell Host Microbe*, 2019, **26**, 15–21.
12 Y. K. Wu, N. C. Cheng and C. M. Cheng, Biofilms in Chronic Wounds: Pathogenesis and Diagnosis, *Trends Biotechnol.*, 2019, **37**, 505–517.
13 K. Lewis, The Science of Antibiotic Discovery, *Cell*, 2020, **181**, 29–45.

 This journal is © The Royal Society of Chemistry 2025

Open Access Article. Published on 06 January 2025. Downloaded on 2/6/2026 5:04:38 PM.
This article is licensed under a Creative Commons Attribution-NonCommercial 3.0 Unported Licence.

14 K. Lewis, R. E. Lee, H. Brötz-Oesterhelt, S. Hiller, M. V. Rodnina, T. Schneider, M. Weingarth and I. Wohlgemuth, Sophisticated Natural Products as Antibiotics, *Nature*, 2024, **632**, 39–49.
15 T. Lluka and J. M. Stokes, Antibiotic Discovery in the Artificial Intelligence Era, *Ann. N. Y. Acad. Sci.*, 2023, **1519**, 74–93.
16 U. Theuretzbacher, B. Blasco, M. Duffey and L. J. V. Piddock, Unrealized Targets in the Discovery of Antibiotics for Gram-negative Bacterial Infections, *Nat. Rev. Drug Discovery*, 2023, **22**, 957–975.
17 B. P. Conlon, E. S. Nakayasu, L. E. Fleck, M. D. LaFleur, V. M. Isabella, K. Coleman, S. N. Leonard, R. D. Smith, J. N. Adkins and K. Lewis, Activated ClpP Kills Persisters and Eradicates a Chronic Biofilm Infection, *Nature*, 2013, **503**, 365–370.
18 L. L. Ling, T. Schneider, A. J. Peoples, A. L. Spoering, I. Engels, B. P. Conlon, A. Mueller, T. F. Schäberle, D. E. Hughes, S. Epstein, M. Jones, L. Lazarides, V. A. Steadman, D. R. Cohen, C. R. Felix, K. A. Fetterman, W. P. Millett, A. G. Nitti, A. M. Zullo, C. Chen and K. Lewis, A New Antibiotic Kills Pathogens without Detectable Resistance, *Nature*, 2015, **517**, 455–459.
19 Y. Imai, K. J. Meyer, A. Iinishi, Q. Favre-Godal, R. Green, S. Manuse, M. Caboni, M. Mori, S. Niles, M. Ghiglieri, C. Honrao, X. Ma, J. J. Guo, A. Makriyannis, L. Linares-Otoya, N. Böhringer, Z. G. Wuisan, H. Kaur, R. Wu, A. Mateus, A. Typas, M. M. Savitski, J. L. Espinoza, A. O'Rourke, K. E. Nelson, S. Hiller, N. Noinaj, T. F. Schäberle, A. D'Onofrio and K. Lewis, A New Antibiotic Selectively Kills Gram-negative Pathogens, *Nature*, 2019, **576**, 459–464.
20 M. G. Charest, C. D. Lerner, J. D. Brubaker, D. R. Siegel and A. G. Myers, A Convergent Enantioselective Route to Structurally Diverse 6-Deoxytetracycline Antibiotics, *Science*, 2005, **308**, 395–398.
21 J. D. Brubaker and A. G. Myers, A Practical, Enantioselective Synthetic Route to a Key Precursor to the Tetracycline Antibiotics, *Org. Lett.*, 2007, **9**, 3523–3525.
22 C. Sun, Q. Wang, J. D. Brubaker, P. M. Wright, C. D. Lerner, K. Noson, M. Charest, D. R. Siegel, Y. M. Wang and A. G. Myers, A Robust Platform for the Synthesis of New Tetracycline Antibiotics, *J. Am. Chem. Soc.*, 2008, **130**, 17913–17927.
23 P. M. Wright, I. B. Seiple and A. G. Myers, The Evolving Role of Chemical Synthesis in Antibacterial Drug Discovery, *Angew. Chem., Int. Ed.*, 2014, **53**, 8840–8869.
24 F. Liu and A. G. Myers, Development of a Platform for the Discovery and Practical Synthesis of New Tetracycline Antibiotics, *Curr. Opin. Chem. Biol.*, 2016, **32**, 48–57.
25 I. Seiple, D. Hog and A. Myers, Practical Protocols for the Preparation of Highly Enantioenriched Silyl Ethers of (*R*,)-3-Hydroxypentan-2-one, Building Blocks for the Synthesis of Macrolide Antibiotics, *Synlett*, 2015, 57–60.
26 Z. Zhang, T. Fukuzaki and A. G. Myers, Synthesis of D-Desosamine and Analogs by Rapid Assembly of 3-Amino Sugars, *Angew. Chem., Int. Ed.*, 2016, **55**, 523–527.
27 I. B. Seiple, Z. Zhang, P. Jakubec, A. Langlois-Mercier, P. M. Wright, D. T. Hog, K. Yabu, S. R. Allu, T. Fukuzaki, P. N. Carlsen, Y. Kitamura, X. Zhou, M. L. Condakes, F. T. Szczypiński, W. D. Green and A. G. Myers, A Platform for the Discovery of New Macrolide Antibiotics, *Nature*, 2016, **533**, 338–345.
28 P. C. Hogan, C. L. Chen, K. M. Mulvihill, J. F. Lawrence, E. Moorhead, J. Rickmeier and A. G. Myers, Large-Scale Preparation of Key Building Blocks for the Manufacture of Fully Synthetic Macrolide Antibiotics, *J. Antibiot.*, 2018, **71**, 318–325.
29 M. J. Mitcheltree, A. Pisipati, E. A. Syroegin, K. J. Silvestre, D. Klepacki, J. D. Mason, D. W. Terwilliger, G. Testolin, A. R. Pote, K. J. Y. Wu, R. P. Ladley, K. Chatman, A. S. Mankin, Y. S. Polikanov and A. G. Myers, A Synthetic Antibiotic Class Overcoming Bacterial Multidrug Resistance, *Nature*, 2021, **599**, 507–512.
30 J. Xie, J. G. Pierce, R. C. James, A. Okano and D. L. Boger, A Redesigned Vancomycin Engineered for Dual D-Ala-D-ala and D-Ala-D-Lac Binding Exhibits Potent Antimicrobial Activity Against Vancomycin-Resistant Bacteria, *J. Am. Chem. Soc.*, 2011, **133**, 13946–13949.
31 J. Xie, A. Okano, J. G. Pierce, R. C. James, S. Stamm, C. M. Crane and D. L. Boger, Total Synthesis of [Ψ[C(═S)NH]Tpg4]Vancomycin Aglycon, [Ψ[C(═NH)NH]Tpg4]Vancomycin Aglycon, and Related Key Compounds: Reengineering Vancomycin for Dual D-Ala-D-Ala and D-Ala-D-Lac Binding, *J. Am. Chem. Soc.*, 2012, **134**, 1284–1297.
32 A. Okano, A. Nakayama, A. W. Schammel and D. L. Boger, Total Synthesis of [Ψ[C(═NH)NH]Tpg$^4$]Vancomycin and its (4-Chlorobiphenyl)methyl Derivative: Impact of Peripheral Modifications on Vancomycin Analogues Redesigned for Dual D-Ala-D-Ala and D-Ala-D-Lac Binding, *J. Am. Chem. Soc.*, 2014, **136**, 13522–13525.
33 A. Okano, A. Nakayama, K. Wu, E. A. Lindsey, A. W. Schammel, Y. Feng, K. C. Collins and D. L. Boger, Total Synthesis and Initial Evaluation of [Ψ[C(═S)NH]Tpg$^4$]Vancomycin, [Ψ[C(═NH)NH]Tpg$^4$]Vancomycin, [Ψ[$CH_2$NH]Tpg$^4$]Vancomycin, and Their (4-Chlorobiphenyl)methyl Derivatives: Synergistic Binding Pocket and Peripheral Modifications for the Glycopeptide Antibiotics, *J. Am. Chem. Soc.*, 2015, **137**, 3693–3704.
34 A. Okano, N. A. Isley and D. L. Boger, Peripheral Modifications of [Ψ[$CH_2$NH]Tpg$^4$]Vancomycin with Added Synergistic Mechanisms of Action Provide Durable and Potent Antibiotics, *Proc. Natl. Acad. Sci. U. S. A.*, 2017, **114**, E5052–E5061.
35 M. F. Richter, B. S. Drown, A. P. Riley, A. Garcia, T. Shirai, R. L. Svec and P. J. Hergenrother, Predictive Compound Accumulation Rules Yield a Broad-Spectrum Antibiotic, *Nature*, 2017, **545**, 299–304.
36 M. F. Richter and P. J. Hergenrother, The Challenge of Converting Gram-positive-Only Compounds into Broad-Spectrum Antibiotics, *Ann. N. Y. Acad. Sci.*, 2019, **1435**, 18–38.
37 S. E. Motika, R. J. Ulrich, E. J. Geddes, H. Y. Lee, G. W. Lau and P. J. Hergenrother, A Gram-negative Antibiotic Active

Open Access Article. Published on 06 January 2025. Downloaded on 2/6/2026 5:04:38 PM.
This article is licensed under a Creative Commons Attribution-NonCommercial 3.0 Unported Licence.

Through Inhibition of an Essential Riboswitch, *J. Am. Chem. Soc.*, 2020, **142**, 10856–10862.

38 E. N. Parker, B. S. Drown, E. J. Geddes, H. Y. Lee, N. Ismail, G. W. Lau and P. J. Hergenrother, Implementation of Permeation Rules Leads to a FabI Inhibitor with Activity Against Gram-negative Pathogens, *Nat. Microbiol.*, 2020, **5**, 67–75.

39 K. A. Munoz and P. J. Hergenrother, Facilitating Compound Entry as a Means to Discover Antibiotics for Gram-negative Bacteria, *Acc. Chem. Res.*, 2021, **54**, 1322–1333.

40 E. J. Geddes, M. K. Gugger, A. Garcia, M. G. Chavez, M. R. Lee, S. J. Perlmutter, C. Bieniossek, L. Guasch and P. J. Hergenrother, Porin-Independent Accumulation in *Pseudomonas* Enables Antibiotic Discovery, *Nature*, 2023, **624**, 145–153.

41 K. A. Muñoz, R. J. Ulrich, A. K. Vasan, M. Sinclair, P. C. Wen, J. R. Holmes, H. Y. Lee, C. C. Hung, C. J. Fields, E. Tajkhorshid, G. W. Lau and P. J. Hergenrother, A Gram-negative-Selective Antibiotic that Spares the Gut Microbiome, *Nature*, 2024, **630**, 429–436.

42 P. A. Smith, M. F. T. Koehler, H. S. Girgis, D. Yan, Y. Chen, Y. Chen, J. J. Crawford, M. R. Durk, R. I. Higuchi, J. Kang, J. Murray, P. Paraselli, S. Park, W. Phung, J. G. Quinn, T. C. Roberts, L. Rougé, J. B. Schwarz, E. Skippington, J. Wai, M. Xu, Z. Yu, H. Zhang, M. W. Tan and C. E. Heise, Optimized Arylomycins are a New Class of Gram-negative Antibiotics, *Nature*, 2018, **561**, 189–194.

43 J. B. Laursen and J. Nielsen, Phenazine Natural Products: Biosynthesis, Synthetic Analogues, and Biological Activity, *Chem. Rev.*, 2004, **104**, 1663–1685.

44 A. Price-Whelan, L. E. P. Dietrich and D. K. Newman, Rethinking "Secondary" Metabolism: Physiological Roles for Phenazine Antibiotics, *Nat. Chem. Biol.*, 2006, **2**, 71–78.

45 N. Guttenberger, W. Blankenfeldt and R. Breinbauer, Recent Developments in the Isolation, Biological Function, Biosynthesis, and Synthesis of Phenazine Natural Products, *Bioorg. Med. Chem.*, 2017, **25**, 6149–6166.

46 Z. A. Machan, T. L. Pitt, W. White, D. Watson, G. W. Taylor, P. J. Cole and R. Wilson, Interaction Between *Pseudomonas aeruginosa* and *Staphylococcus aureus*: Description of an Antistaphylococcal Substance, *J. Med. Microbiol.*, 1991, **34**, 213–217.

47 N. V. Borrero, F. Bai, C. Perez, B. Q. Duong, J. R. Rocca, S. Jin and R. W. Huigens III, Phenazine Antibiotic Inspired Discovery of Potent Bromophenazine Antibacterial Agents against *Staphylococcus aureus* and *Staphylococcus epidermidis*, *Org. Biomol. Chem.*, 2014, **12**, 881–886.

48 A. T. Garrison, Y. Abouelhassan, D. Kallifidas, F. Bai, M. Ukhanova, V. Mai, S. Jin, H. Luesch and R. W. Huigens, Halogenated Phenazines That Potently Eradicate Biofilms, MRSA Persister Cells in Non–Biofilm Cultures, and *Mycobacterium tuberculosis*, *Angew. Chem., Int. Ed.*, 2015, **54**, 14819–14823.

49 A. T. Garrison, Y. Abouelhassan, V. M. Norwood, D. Kallifidas, F. Bai, M. T. Nguyen, M. Rolfe, G. M. Burch, S. Jin, H. Luesch and R. W. Huigens, Structure–Activity Relationships of a Diverse Class of Halogenated Phenazines that Targets Persistent, Antibiotic-Tolerant Bacterial Biofilms and *Mycobacterium tuberculosis*, *J. Med. Chem.*, 2016, **59**, 3808–3825.

50 H. Yang, Y. Abouelhassan, G. M. Burch, D. Kallifidas, G. Huang, H. Yousaf, S. Jin, H. Luesch and R. W. Huigens, A Highly Potent Class of Halogenated Phenazine Antibacterial and Biofilm-Eradicating Agents Accessed Through a Modular Wohl-Aue Synthesis, *Sci. Rep.*, 2017, **7**, 2003.

51 Y. Abouelhassan, Y. Zhang, S. Jin and R. W. Huigens III, Transcript Profiling of MRSA Biofilms Treated with a Halogenated Phenazine Eradicating Agent: A Platform for Defining Cellular Targets and Pathways Critical to Biofilm Survival, *Angew. Chem., Int. Ed.*, 2018, **57**, 15523–15528.

52 A. T. Garrison, Y. Abouelhassan, D. Kallifidas, H. Tan, Y. S. Kim, S. Jin, H. Luesch and R. W. Huigens, An Efficient Buchwald–Hartwig/Reductive Cyclization for the Scaffold Diversification of Halogenated Phenazines: Potent Antibacterial Targeting, Biofilm Eradication, and Prodrug Exploration, *J. Med. Chem.*, 2018, **61**, 3962–3983.

53 H. Yang, S. Kundra, M. Chojnacki, K. Liu, M. A. Fuse, Y. Abouelhassan, D. Kallifidas, P. Zhang, G. Huang, S. Jin, Y. Ding, H. Luesch, K. H. Rohde, P. M. Dunman, J. A. Lemos and R. W. Huigens, A Modular Synthetic Route Involving *N*-Aryl-2-Nitrosoaniline Intermediates Leads to a New Series of 3-Substituted Halogenated Phenazine Antibacterial Agents, *J. Med. Chem.*, 2021, **64**, 7275–7295.

54 K. Liu, M. Brivio, T. Xiao, V. M. Norwood, Y. S. Kim, S. Jin, A. Papagni, L. Vaghi and R. W. Huigens, Modular Synthetic Routes to Fluorine-Containing Halogenated Phenazine and Acridine Agents That Induce Rapid Iron Starvation in Methicillin-Resistant *Staphylococcus aureus* Biofilms, *ACS Infect. Dis.*, 2022, **8**, 280–295.

55 T. Xiao, K. Liu, Q. Gao, M. Chen, Y. S. Kim, S. Jin, Y. Ding and R. W. Huigens III, Design, Synthesis and Evaluation of Carbonate-Linked Halogenated Phenazine-Quinone Prodrugs with Improved Water-Solubility and Potent Antibacterial Profiles, *ACS Infect. Dis.*, 2023, **9**, 899–915.

56 T. Fu, Z. Cai, Z. Yue, H. Yang, B. Fang, X. Zhang, Z. Fan, X. Pan, F. Yang, Y. Jin, Z. Cheng, W. Wu, B. Sun, R. W. Huigens, L. Yang and F. Bai, Evolution of Resistance to Phenazine Antibiotics in *Staphylococcus aureus* and Its Role During Coinfection with *Pseudomonas aeruginosa*, *ACS Infect. Dis.*, 2021, **7**, 636–649.

57 Z. Wróbel and A. Kwast, 2-Nitroso-*N*-arylanilines: Products of Acid-Promoted Transformation of σH Adducts of Arylamines and Nitroarenes, *Synlett*, 2007, 1525–1528.

58 Z. Wróbel and A. Kwast, Simple Synthesis of *N*-Aryl-2-nitrosoanilines in the Reaction of Nitroarenes with Aniline Anion Derivatives, *Synthesis*, 2010, 3865–3872.

59 A. Kwast, K. Stachowska, A. Trawczyński and Z. Wróbel, *N*-Aryl-2-Nitrosoanilines as Intermediates in the Synthesis of Substituted Phenazines from Nitroarenes, *Tetrahedron Lett.*, 2011, **52**, 6484–6488.

 This journal is © The Royal Society of Chemistry 2025

Open Access Article. Published on 06 January 2025. Downloaded on 2/6/2026 5:04:38 PM.
This article is licensed under a Creative Commons Attribution-NonCommercial 3.0 Unported Licence.

60 Z. Wróbel, K. Plichta and A. Kwast, Reactivity and Substituent Effects in the Cyclization of *N*-Aryl-2-nitrosoanilines to Phenazines, *Tetrahedron*, 2017, **73**, 3147–3152.

61 K. Liu, T. Xiao, H. Yang, M. Chen, Q. Gao, B. R. Brummel, Y. Ding and R. W. Huigens III, Design, Synthesis and Evaluation of Halogenated Phenazine Antibacterial Prodrugs Targeting Nitroreductase Enzymes for Activation, *RSC Med. Chem.*, 2023, **14**, 1472–1481.

62 H. Ceri, M. E. Olson, C. Stremick, R. R. Read, D. Morck and A. Buret, The Calgary Biofilm Device: New Technology for Rapid Determination of Antibiotic Susceptibilities of Bacterial Biofilms, *J. Clin. Microbiol.*, 1999, **37**, 1771–1776.

63 J. J. Harrison, C. A. Stremick, R. J. Turner, N. D. Allan, M. E. Olson and H. Ceri, Microtiter Susceptibility Testing of Microbes Growing on Peg Lids: A Miniaturized Biofilm Model for High-Throughput Screening, *Nat. Protoc.*, 2010, **5**, 1236–1254.

64 M. C. Jennings, L. E. Ator, T. J. Paniak, K. P. C. Minbiole and W. M. Wuest, Biofilm-Eradicating Properties of Quaternary Ammonium Amphiphiles: Simple Mimetics of Antimicrobial Peptides, *ChemBioChem*, 2014, **15**, 2211–2215.

65 *Methods for dilution antimicrobial susceptibility tests for bacteria that grow aerobically; approved standards*, Clinical and Laboratory Standards Institute, Wayne, PA, 8th edn (M7–M8), 2009.

66 F. C. Rodrigues, R. Gupta, S. Geden, J. Roberts, P. Winder, S. A. Pomponi, M. C. Diaz, J. K. Reed, A. E. Wright and K. H. Rohde, Selective Killing of Dormant *Mycobacterium tuberculosis* by Marine Natural Products, *Antimicrob. Agents Chemother.*, 2017, **61**, e00743–e00717.

67 C. Deb, C. M. Lee, V. S. Dubey, J. Daniel, B. Abomoelak, T. D. Sirakova, S. Pawar, L. Rogers and P. E. Kolattukudy, A Novel *In Vitro* Multiple-Stress Dormancy Model for *Mycobacterium tuberculosis* Generates a Lipid-Loaded, Drug-Tolerant, Dormant Pathogen, *PLoS One*, 2009, **4**, e6077.

68 Y. Y. Pang, J. Schwartz, M. Thoendel, L. W. Ackermann, A. R. Horswill and W. M. Nauseef, agr-Dependent Interactions of *Staphylococcus aureus* USA300 with Human Polymorphonuclear Neutrophils, *J. Innate Immun.*, 2010, **2**, 546–559.